Intravoxel Incoherent Motion in Body Diffusion-Weighted MRI: Reality and Challenges

Dow-Mu Koh[1]
David J. Collins[1,2]
Matthew R. Orton[2]

OBJECTIVE. Diffusion-weighted MRI is increasingly applied in the body. It has been recognized for some time, on the basis of scientific experiments and studies in the brain, that the calculation of apparent diffusion coefficient by simple monoexponential relationship between MRI signal and b value does not fully account for tissue behavior. However, appreciation of this fact in body diffusion MRI is relatively new, because technologic advancements have only recently enabled high-quality body diffusion-weighted images to be acquired using multiple b values. There is now increasing interest in the radiologic community to apply more sophisticated analytic approaches, such as those based on the principles of intravoxel incoherent motion, which allows quantitative parameters that reflect tissue microcapillary perfusion and tissue diffusivity to be derived.

CONCLUSION. In this review, we discuss the principles of intravoxel incoherent motion as applied to body diffusion-weighted MRI. The evidence for the technique in measuring tissue perfusion is presented and the emerging clinical utility surveyed. The requisites and challenges of quantitative evaluation beyond simple monoexponential relationships are highlighted.

In the 1980s, the use of clinical diffusion-weighted (DW) MRI was largely confined to the brain for the early detection of cerebral infarction. However, technologic innovations in the last decade, such as improved MRI gradient performance, multichannel surface receiver coils, parallel imaging techniques, and improved fat suppression schemes, have facilitated the translation of such measurements to the body [1]. Applying these technologies enabled high-quality DW-MRI scans to be obtained in free-breathing, which helped to conceptualize the whole-body DW imaging with background signal suppression technique [2].

Because quantitative imaging is likely to grow in scope and importance, the radiologic community has embraced the potential of DW-MRI, such that there is now a steady stream of publications on its use in the body for oncologic and nononcologic applications. The technique enables the calculation of tissue apparent diffusion coefficient (ADC), a quantitative measure of tissue diffusivity. This makes it possible to objectively compare results, such as when evaluating tumor ADC before and after chemotherapy to identify treatment response.

However, it has been recognized for some time that the calculated ADC value is sensitive to capillary perfusion, which represents bulk motion of intravascular water protons within imaging voxels [3–6]. In 1986, Le Bihan et al. [3] proposed the principles of intravoxel incoherent motion (IVIM) and suggested that using a more sophisticated approach to describe the relationship between signal attenuation in tissues with increasing b value would enable quantitative parameters that separately reflect tissue diffusivity and tissue microcapillary perfusion to be estimated. There is growing interest in applying analytic techniques beyond simple ADC calculations to tease out the effects of microcapillary perfusion from DW-MRI data [7]. This is driven by the realization that the assumption of a simple exponential relationship between signal attenuation and b value for ADC calculation is simplistic and by the perceived value of obtaining perfusion-related data from a relatively simple measurement. However, to do this in a meaningful way demands insight into the approach and a clear understanding of the strengths and limitations of the method.

This article is aimed at radiologists and technologists who are currently engaged in

Keywords: diffusion, MRI, oncology, perfusion

DOI:10.2214/AJR.10.5515

Received August 10, 2010; accepted after revision December 15, 2010. Supported by the Cancer Research UK and EPSRC Cancer Imaging Centre in association with the MRC and Department of HEalth (England) grant C1060/A10334 and National Health Service funding to the NIHR Biomedical Research Centre.

[1]Department of Radiology, Royal Marsden Hospital, Downs Rd, Sutton SM2 5PT, UK. Address correspondence to D. M. Koh.

[2]Cancer Research UK-EPSRC Cancer Imaging Centre, Institute of Cancer Research, Sutton, UK.

AJR 2011; 196:1351–1361

0361–803X/11/1966–1351

applying DW-MRI in the body for disease evaluation and who are interested in extending the quantitative potential of the technique in their practice or research. In this review, the principles of IVIM are discussed and the published literature surveyed to examine the link between quantitative parameters derived by IVIM-based analysis and vascular perfusion. The emerging extracranial applications of IVIM DW-MRI in clinical studies are examined, focusing on the potential of such analysis to inform about disease states. Finally, we will highlight challenges of implementing such complex data acquisition and analysis. The basic principles of DW-MRI are assumed and will only be briefly discussed. The reader should refer elsewhere for a more comprehensive discussion of the basic principles of DW-MRI [1, 8].

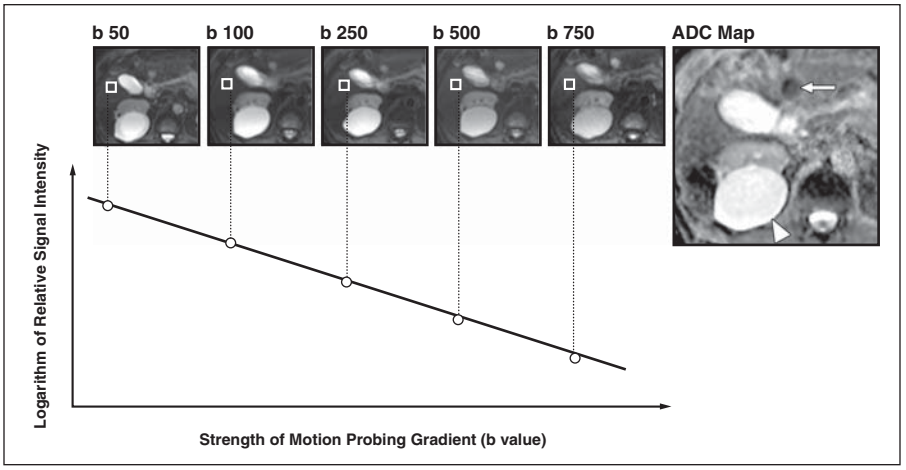

Fig. 1—Apparent diffusion coefficient (ADC) calculation. Simplified scheme shows ADC calculation from b value diffusion-weighted imaging. For each image voxel acquired at same anatomic position at increasing b value, logarithm of relative signal intensity is plotted against b value. Slope of line (monoexponential fit) is ADC of that image voxel. Process is repeated for every voxel on image, and ADC values of all voxels can be displayed as parametric ADC map. In this example, metastasis in left lobe of liver (*arrow*) returns low ADC, indicating relatively impeded water diffusion, whereas cyst in right kidney (*arrowhead*) returns high ADC. Note that cyst also shows high signal on b value images due to relatively long T2 relaxation time, phenomenon known as "T2-shine through."

Understanding DW-MRI and IVIM

DW-MRI is sensitive to the thermally driven random motion of water protons, which is modified in tissues by their interactions with cell membranes and macromolecules. Thus, the apparent diffusion of water in tissues reflects tissue cellularity, the tortuosity of the extracellular space, integrity of cell membranes, and viscosity of fluids [1]. Stejskal and Tanner [9] described a spin-echo MRI experiment that can be used to measure water diffusion and remains the basis for many body DW-MRI sequences in use today.

Calculation of ADC From DW-MRI Measurements

By performing DW-MRI with at least two diffusion weightings, or b values, the differential signal attenuation at different b values can be used to calculate the ADC. In its simplest form, the slope of the line that describes the relationship between the logarithm of the signal intensity and the b value is the ADC (Fig. 1). If the calculation is repeated for each voxel of the DW-MRI, then the ADC value for every image voxel can be derived and displayed as a parametric ADC map. Thus, voxels that show a steeper slope of signal attenuation with increasing b values will have higher ADC values (indicating higher water diffusivity) compared with voxels that show a gradual slope of signal attenuation. Cellular tissues (e.g., tumor tissues) in the body often return lower ADC values compared with native tissues, which facilitates their detection and characterization. The ADC is usually expressed in units of 10^{-3} mm^2/s. Although an ADC map may be generated under optimal measurement conditions by using just two b values, using more than two b values at image acquisition generally gives more accurate ADC values, especially where the likely ADC values are not known a priori.

Microcapillary Perfusion: Implications for DW-MRI Measurements and ADC Calculations

When DW-MRI is performed in well-perfused body tissues within the b value range usually applied for body imaging (i.e., 0–1000 s/mm^2), the measured signal attenuation at low b values (e.g., 0–100 s/mm^2) arises not only from water diffusion in tissues but also from microcirculation within the normal capillary network. Both these processes result in phase dispersion at DW-MRI, leading to signal attenuation. Le Bihan et al. [3] termed the behavior of protons that display signal attenuation at DW-MRI as showing IVIM.

Microcirculatory perfusion of blood within capillaries has no specific orientation and can therefore be thought of as a type of "pseudodiffusion," which depends on the velocity of the flowing blood and the vascular architecture. The effect of pseudodiffusion on the signal attenuation in each imaging voxel is also b value dependent. However, the rate of signal attenuation resulting from pseudodiffusion is typically an order of magnitude greater than tissue diffusion because of larger distances of proton displacement during the application of the motion-probing gradients. Therefore, in normal perfused tissue at higher b values, pseudodiffusion accounts for only a small proportion (if any) of the measured signal in each imaging voxel. However, at lower b values, this relative contribution to the DW-MRI signal becomes significant.

A plot of the signal attenuation of a well-perfused tissue (liver parenchyma) with increasing b values from a healthy individual is shown in Figure 2. Not surprisingly, protons associated with flowing blood have relatively large diffusion distances, and the signal is suppressed by small diffusion weightings (e.g., b value ≤ 100 s/mm^2). Thus, there is a steeper slope of signal attenuation for b values near zero, which can be attributed to microcapillary perfusion. By contrast, larger b values are less sensitive to contributions from microcapillary perfusion because the signal attenuation of the perfusing protons is essentially complete. At larger b values (e.g., > 100 s/mm^2), the slope of signal attenuation is less steep, which is more reflective of tissue diffusivity. Hence, in this example, a line drawn to best fit all the data points has the shape of a hockey stick, which is described by the IVIM model. The IVIM approach uses a biexponential function to describe the DW-MRI data and makes the assumption that the measured signal attenuation at DW-MRI comprises a mixture of tissue perfusion and tissue diffusivity effects. Using IVIM-based analysis, it is possible to derive other quantitative indexes that describe tissue water diffusivity, tissue perfusion (pseudodiffusion coefficient), and

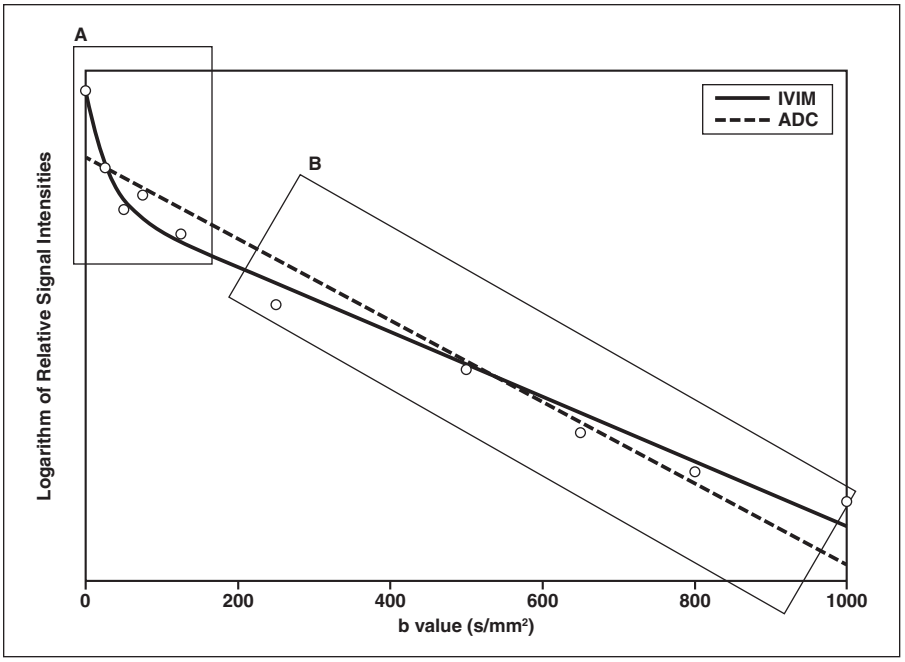

Fig. 2—Healthy 30-year-old man. Plots show logarithm of relative signal intensity versus b value from normal liver parenchyma. Note that there is initially steeper decrease in plotted signal values (*circles*) at low b values (within rectangular box A) compared with more gradual attenuation of signal at higher b values (within rectangular box B). By applying intravoxel incoherent motion (IVIM) analysis, biexponential behavior of signal attenuation is characterized (*solid line*), resulting in typical hockey stick appearance of fitted curve. Using simple monoexponential apparent diffusion coefficient (ADC) line fitted to data (*dotted line*) in this case provides suboptimal characterization of signal attenuation behavior.

the perfusion fraction of tissues, which can also be displayed as parametric maps (Fig. 3). In this review, the IVIM analysis and graphical plots are averaged over entire regions of interest and are computed using a method described by Neil and Bretthorst [10]. However, other mathematic methods can be applied to do this, but a discussion of these methods is beyond the scope of this review.

Currently, on most commercial MRI systems, the ADC value is calculated automatically and by default using all available b value images with a monoexponential function (e.g., a straight line fit to the logarithm of signal intensity versus b value) (Fig. 2). Thus, depending on the range and number of b values used at imaging, the calculated ADC by this approach is, to various extents, influenced by microcapillary perfusion.

From the above discussion, it should be clear, therefore, that the ADC value of perfused tissues calculated from only low b value images (e.g., ≤ 100 s/mm^2, sometimes referred to as ADC_{low}) would be perfusion sensitive, whereas the ADC value calculated from images of higher b values (e.g., > 100 s/mm^2, sometimes referred to as ADC_{high}) and excluding lower b values would be relatively perfusion insensitive. It can also be reasoned that ADC_{high} values are likely to be very similar to the diffusion coefficient derived by IVIM-based analysis for any particular tissue (Fig. 3). It is also worthwhile remembering that, although ADC_{low} is perfusion sensitive, it is also affected by diffusion effects in tissues.

Evidence for Tissue Perfusion Using DW-MRI Measurements

There are experimental and clinical data to support the biexponential behavior of signal at-

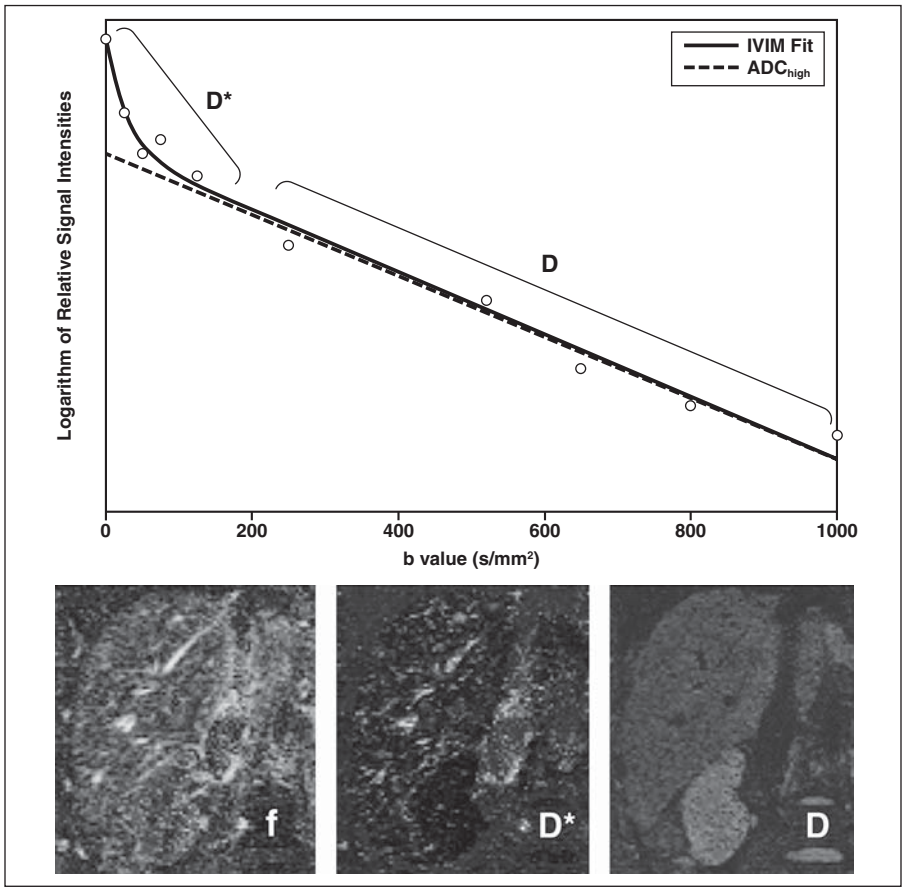

Fig. 3—Healthy 30-year-old man. Diffusion-weighted MRI of liver was performed in coronal plane. By applying intravoxel incoherent motion (IVIM)–based biexponential analysis of normal liver, different parts of signal attenuation curve (*solid line*) for each image voxel are closely linked to estimated quantitative parameters of diffusion coefficient (D), which reflects tissue diffusivity; pseudodiffusion coefficient (D*), which reflects microcapillary perfusion; and perfusion fraction (f). Results for all voxels are displayed as parametric maps as shown. Note also that apparent diffusion coefficient value calculated from images using only higher b values (> 100 s/mm^2) (ADC_{high}) will approximate D, because they have similar gradients.

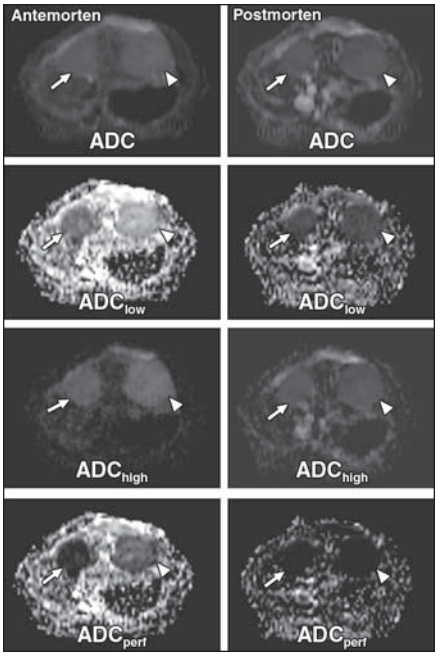

Fig. 4—Diffusion-weighted MRI in rat with two implanted rhabdomyosarcoma tumors (*arrow* and *arrowhead*, all panels) performed antemortem and postmortem. Parametric maps of apparent diffusion coefficient (ADC) were generated using all b values (0, 50, 100, 150, 200, 250, 300, 500, 750, and 1000 s/mm^2), ADC$_{low}$ using b values of 0, 50, and 100 s/mm^2; ADC$_{high}$ using b values of 500, 750, and 1000 s/mm^2; and ADC$_{perf}$ calculated as ADC$_{low}$ – ADC$_{high}$. Note that ADC$_{low}$ maps revealed tumor values (*arrow* and *arrowhead*) to be higher in antemortem state compared with postmortem state, in keeping with effects of microcapillary perfusion, whereas ADC$_{high}$ maps, which are perfusion insensitive, appeared similar. Subtraction maps (ADC$_{perf}$) in antemortem state showed perfusion fraction within tumors but this was not observed postmortem. (Courtesy of Ni Y and De Keyzer F, University of Leuven, Leuven, Belgium)

tenuation observed in body tissues at DW-MRI and that indicate the signal attenuation observed at low b values is related to tissue perfusion.

Phantom Studies

Le Bihan et al. [4] used a phantom that could show the effects of perfusion using DW imaging. This included a chromatographic column packed with resin microspheres (Sephadex G100, Sigma-Aldrich) through which water percolates under gravity. Protons within the microspheres showed only diffusion, whereas water in the spaces between microspheres was reasoned to show flow analogous to microcapillary perfusion. DW-MRI was performed on the phantom using six b values, and water flow through the resin column varied. It was shown that reducing water flow through the resin column resulted in a decrease in the measured ADC and perfusion fraction calculated by biexponential fitting of the data [4]. This indicates that DW-MRI measurement is sensitive to flow effects.

Preclinical and Clinical Studies

A number of preclinical studies have compared ADC obtained in living versus postmortem animals to show the influence of tissue perfusion on ADC [11, 12]. Sakuma et al. [11] using implanted human tumors in nude mice showed that the measured ADC in tumors was significantly higher in living mice compared with mice that were sacrificed. In another study, Sun et al. [12] calculated perfusion-sensitive ADCs (using b values of 0–100 s/mm^2) and perfusion-insensitive ADCs (using b values of 500–1000 s/mm^2) in rat livers implanted with rhabdomyosarcoma in living and postmortem animals. They found the perfusion-sensitive ADC significantly decreased in tumors and normal liver in the postmortem state, but no significant change was observed in the perfusion-insensitive ADC (Fig. 4).

Other studies have modulated vascular flow in living animals to observe changes in diffusion measurements. Neil et al. [13] and Henkelman et al. [14] altered cerebral blood flow in rat brains by increasing the arterial carbon dioxide concentrations, leading to increased cerebral perfusion. They found that the perfusion parameters (pseudodiffusion coefficient and perfusion fraction) by IVIM-based analysis were correlated with the arterial carbon dioxide concentrations. Wang et al. [15] increased blood flow in a mammary adenocarcinoma rat model by administering the vasodilator hydralazine. Injection of IV hydralazine increased tumor blood flow, which was accompanied by a measurable increase in the IVIM-derived pseudodiffusion coefficient. In another study, a dog kidney was excised, isolated, and perfused using a mechanical pump [16]. On DW-MRI, the ADC and perfusion fraction of the kidney increased as flow through the kidney was increased by the mechanical pump, but tissue diffusivity showed no significant change. In a recent clinical study [17], the perfusion fraction in normal pancreatic tissue was reduced by suppression of flow at low b values, but the diffusion coefficient was unchanged. These studies show that DW-MRI measurements are sensitive to tissue perfusion, and the technique could thus be potentially harnessed to provide assessment of the microcirculatory perfusion of tissues, in addition to measuring tissue diffusivity.

Relationship Between Microcapillary Perfusion Measured by DW-MRI and Perfusion Measured by Other Imaging Techniques

In theory, there should be close agreement between perfusion quantified by DW-MRI and perfusion evaluated by other techniques. Henkelman [18] argued that perfusion measured by DW-MRI could be different from perfusion measured using intravascular tracers (e.g., contrast medium) because such perfusion estimates were based on tissue uptake or removal of the injected tracer. However, Le Bihan and Turner [19] reasoned that, even with the use of freely diffusible tracers, the delivery of tracer to tissues is still dependent on intravascular flow and there is thus highly likely to be a relationship between tissue perfusion measured using DW-MRI and tissue perfusion measured using tracer kinetic methods.

In the published literature, DW-MRI–derived perfusion indexes have been reported to correlate with perfusion parameters derived using other techniques. One study [20] in the brains of 28 volunteers compared IVIM-based analysis with relative blood flow and relative blood volume obtained by dynamic susceptibility contrast enhancement imaging. The perfusion fraction was correlated with the relative blood volume, and the pseudodiffusion coefficient was correlated with the relative blood flow. In another study in patients with renal artery stenosis [21], relative blood flow determined by radionuclide tracer technique was found to correlate with the ADC.

However, perhaps not surprisingly, no clear relationship could be found between DW-MRI–derived parameters and perfusion derived using other techniques on other occasions [22]. One of the likely reasons is because the "fast component," or perfusion fraction measured by DW-MRI, may comprise more than one physiologic process (e.g., glandular secretion and ductal flow). Evidence that this is likely has been shown by increase in ADC of normal salivary glands in response to gustatory stimulation [23, 24]. These bulk flow phenomena will also contribute to the signal attenuation measured at low b values and will be difficult, if not impossible, to isolate from microcapillary perfusion effects. For these reasons, doubt was expressed by Muller et al. [25] as to whether IVIM evaluation could measure true vascular perfusion in kidneys. They argued that the lack of a clear strong bi-exponential signal decay in the kidney and the relatively small difference between the measured cortical and medullary ADC suggest

TABLE 1: Summary of Diffusion-Weighted (DW) MRI Studies Using Quantitative Indexes Beyond Simple Monoexponential Apparent Diffusion Coefficient (ADC) Evaluation

Study	No. of Patients	Organ	b Values (s/mm^2)	Findings
Shinmoto et al. [32]	22	Prostate	0–3000 in 16 steps	ADC_{high} and ADC_{low} values of cancers were significantly lower than transitional or peripheral zones. Fraction of ADC_{low} component was significantly smaller in cancer than in peripheral zone.
Mulkern et al. [31]	9	Prostate	5–3500 in 14 steps	Signal attenuation in prostate was better described using bi- vs monoexponential fits. Difference between ADC_{high} within central gland and peripheral zone was statistically significant.
Riches et al. [30]	50	Prostate	0, 1, 2, 4, 10, 20, 50, 100, 200, 400, and 800	Biexponential model best described data when low b values were included, suggesting a perfusion component. Perfusion coefficients and fractions were highly variable within population.
Lemke et al. [33]	23 (and 14 volunteers)	Pancreas	0–800 in 11 steps	Lower perfusion fraction in pancreatic cancer was the best parameter for differentiating healthy pancreas from pancreatic cancer.
Yamada et al. [34]	78	Liver	30, 300, 900, and 1100	ADCs of solid organs and solid lesions were significantly higher than their diffusion coefficient values, indicating contribution of perfusion to the ADCs.
Koh et al. [35]	40	Liver	0, 150, and 500	Metastases showed lower estimated perfusion fraction compared with liver parenchyma.
Luciani et al. [49]	12 (and 25 volunteers)	Liver	0, 10, 20, 30, 50, 80, 100, 200, 400, and 800	Mean ADC values were significantly higher than diffusion coefficient in healthy liver group and in cirrhotic liver group. ADC and pseudodiffusion coefficients were significantly reduced in cirrhotic liver compared with healthy liver.
Eisenberger et al. [37]	15	Renal transplant	0, 10, 20, 50, 100, 180, 300, 420, 550, and 700	Perfusion fraction values were significantly reduced to less than 12% in cortex and medulla of renal transplants with acute rejection and acute tubular necrosis. Perfusion fraction values correlated with creatinine clearance.
Zhang et al. [38]	3 (and metaanalysis)	Renal	16 b values ≤ 750; 27 b values 0–1300	Use of a monoexponential fit for DW-MRI data and variably sampled diffusion weightings play a substantial role in ADC variations reported in healthy kidneys.
Thoeny et al. [26]	15 (and 18 volunteers)	Renal	0, 50, 100, 500, 750, and 1000	Perfusion insensitive ADC_{high} was significantly higher in cortex than medulla. No difference between cortex and medulla was observed for perfusion-sensitive ADC_{low}.
Thoeny et al. [36]	15 (and 15 control subjects)	Renal	0, 10, 20, 40, 60, 150, 300, 500, 700, and 900	ADC, diffusion coefficient, and perfusion fraction were similar in cortex and medulla of transplanted kidneys. In healthy volunteers, values in medulla were similar to those in cortex and medulla of patients, but values in cortex were higher than medulla of healthy individuals.
Kwee et al. [47]	20	Glioma	0, 1000, 2000, and 4000	Stretched exponential used for model fitting. Mean heterogeneity index of tumors was significantly lower than contralateral normal frontal white matter.

that the generally high diffusion values encountered in the kidneys (typically about 2×10^{-3} mm^2/s) [26] may be more related to other flow-dependent transport mechanisms (e.g., renal tubular flow) rather than renal vascular perfusion. Even if vascular flow does contribute to the signal attenuation measured in the kidneys, it is currently not possible to isolate the signal contribution of vascular flow from renal tubular flow by IVIM analysis. Clearly, more work is needed to verify the physiologic basis for the DW-MRI measurements in functionally complex organs. Nevertheless, most recent studies have shown that the measured ADC of the normal renal cortex is higher than that of the medulla [26–29], suggesting that perfusion is still a probable contributor to the observed difference.

Clinical Applications of DW-MRI for Extracting Perfusion-Related Information

Despite some uncertainties with regard to the physiologic basis of DW-MRI observations that relate to tissue perfusion, clinical application of these techniques has yielded interesting results. These studies are summarized in Table 1.

It was found that the signal attenuation of the prostate gland with increasing b value conformed to a biexponential behavior [30, 31]. Both the fast (pseudodiffusion) and slow component (tissue diffusivity) of diffusion were reportedly lower in prostate cancer compared with normal peripheral or transitional zones [32].

In the pancreas, the identification of pancreatic carcinoma and distinguishing between tumor and focal pancreatitis still pose

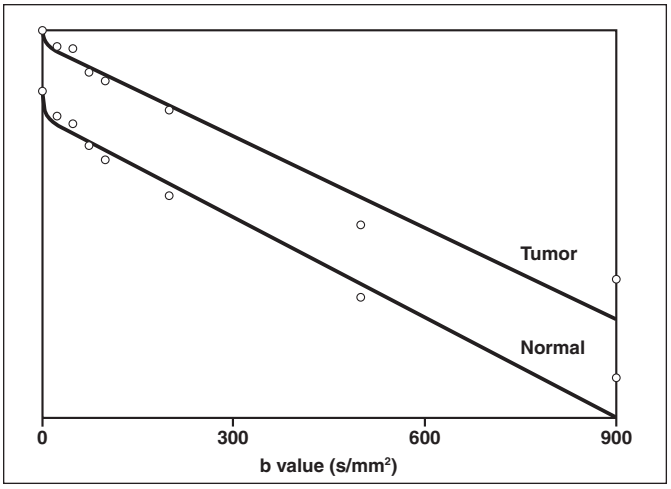

A

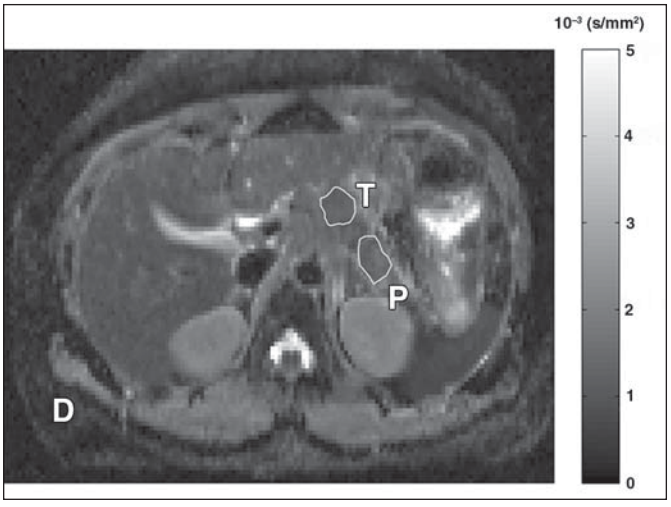

B

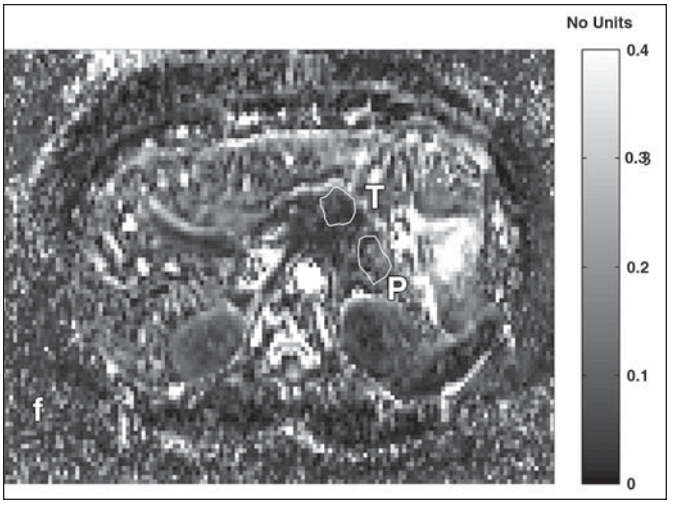

C

Fig. 5—54-year-old man with biopsy-proven adenocarcinoma of pancreas. **A,** Axial scans were performed using navigator-controlled spin-echo echo-planar diffusion-weighted MRI with eight b values (0, 25, 50, 75, 100, 250, 500, and 900 s/mm^2). Mean signal attenuation curves by intravoxel incoherent motion–based analysis of pancreatic tumor and normal pancreatic tissue with increasing b value are shown with offset in vertical axis for data display. **B** and **C,** Parametric maps of diffusion coefficient (D) (**B**) and perfusion fraction (f) (**C**). Positions of tumor (T) and normal pancreas (P) are indicated by regions of interest. There is slight difference in mean diffusion coefficient of tumor compared with normal pancreas (1.30×10^{-3} vs 1.44×10^{-3} mm^2/s). However, perfusion fraction is reduced within tumor compared with normal pancreas (0.06 vs 0.10). Note "flattening" of mean signal attenuation curve at low b values in tumor suggesting lower perfusion compared with normal pancreas.

significant diagnostic challenges. In a recent study [33], the perfusion fraction of pancreatic carcinoma was shown to be significantly lower than and showed little overlap with normal pancreatic parenchyma (Fig. 5). These results suggest that the perfusion fraction could be helpful to identify and characterize pancreatic malignancy.

In the abdomen, IVIM DW-MRI [34] of intraabdominal organs, such as the liver, spleen, and kidneys (Fig. 6), revealed a biexponential pattern of signal attenuation. Using the IVIM model, the calculated ADC values using all b values of these organs were significantly higher than the corresponding tissue diffusion coefficients. In colorectal liver metastases [35], the estimated perfusion fraction of colorectal liver metastases was lower than that in normal liver parenchyma, in keeping with the hypovascular nature of these lesions (Fig. 7). More recently, IVIM analysis in patients with liver cirrhosis found that the pseudoperfusion coefficient and the ADC of the liver were both lower in cirrhotic liver than in normal liver.

The diffusion coefficient and the perfusion fraction were reportedly higher in the cortex compared with the medulla in normal kidneys [36]. However, this differentiation was lost in renal transplant allograft [36] (Fig. 8). Interestingly, the perfusion fraction could be correlated with creatinine clearance [36, 37], suggesting that the technique has the potential to noninvasively assess the renal function. Applying a biexponential model was also shown to reduce errors in ADC quantifications across the whole kidney, within the renal cortex or the medulla [38].

These clinical studies show the evolving utility of the perfusion-sensitive component of diffusion to inform on disease states. However, such data are only beginning to emerge. Critically, such analysis cannot yet be performed using standard vendor software that only applies a simple monoexponential fit to all b values data. However, before such an analytic approach can be generalized, it is important to reflect on some of the challenges that need to be addressed.

Challenges to Implementation of Biexponential Fitting of DW-MRI Data

There is recognition that using monoexponential fitting of DW-MRI data in the body can be an important source of variation in reported ADC measurements [38]. However, it is important to remember that, for any quantitative metric to be useful, the process of image acquisition, image processing, model fitting to the acquired data, and analysis of parametric maps will need to be sufficiently robust so that accurate and reproducible measurements can be made to yield biologically relevant and

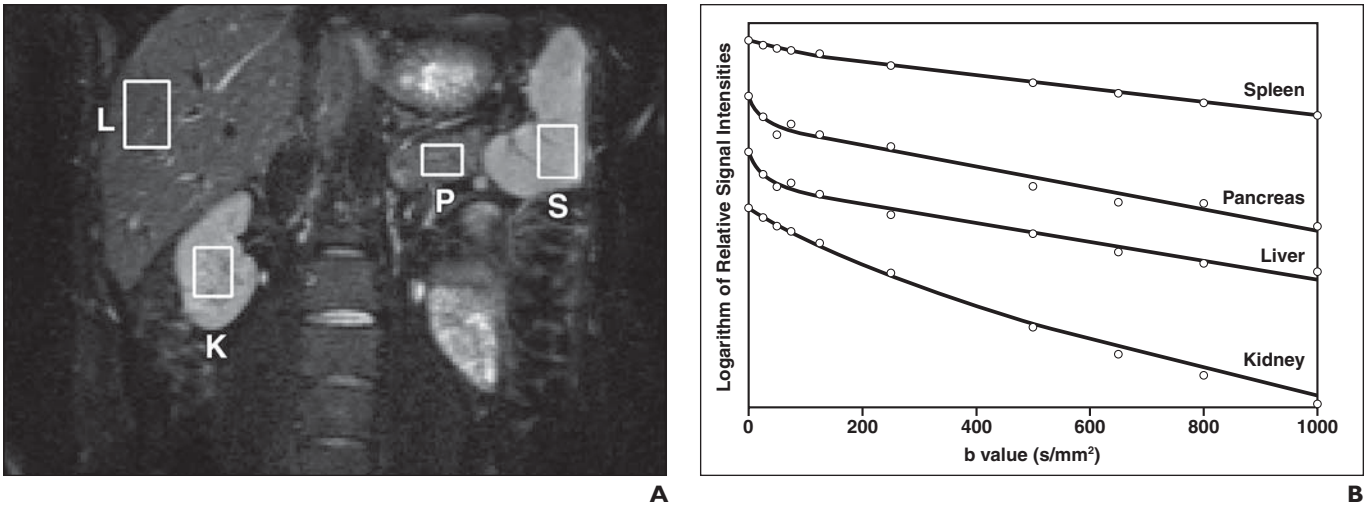

Fig. 6—Signal attenuation behavior of abdominal viscera at diffusion-weighted (DW) MRI in healthy 30-year-old man.
A, Coronal DW-MRI scan (b = 0 s/mm^2) shows rectangular regions of interest drawn over liver (L), right kidney (K), pancreas (P), and spleen (S).
B, Mean curves by intravoxel incoherent motion–based analysis displayed with offset in vertical axis showing attenuation of signal intensities within these organs at b values of 0, 25, 50, 75, 100, 150, 250, 500, 650, 800, and 1000 s/mm^2. Note that curves from liver and pancreas have hockey stick appearance typical of biexponential behavior, with transition between two components observed at low b values (< 100 s/mm^2). However, this is not obvious within spleen or kidney.

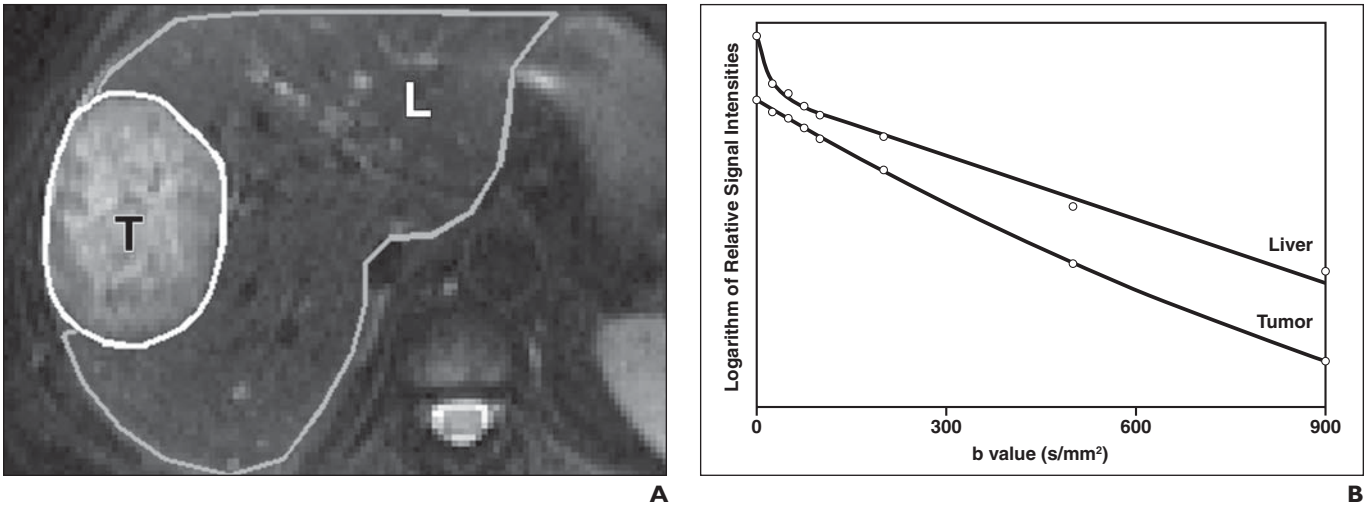

Fig. 7—45-year-old man with colorectal liver metastasis to right lobe of liver.
A, Axial diffusion-weighted MRI scan (b = 0 s/mm^2) shows regions of interest drawn over tumor (T) and normal liver (L). Note high signal centrally within metastasis suggesting necrosis.
B, Mean signal attenuation curves by intravoxel incoherent motion biexponential analysis shows typical behavior of liver, with significant perfusion fraction. By contrast, signal attenuation curve for metastasis is relatively flat at low b values suggesting low perfusion fraction. This observation is in keeping with known pathology of colorectal liver metastases, which are usually hypovascular compared with normal liver parenchyma.

clinically meaningful results. Applied inappropriately, quantitative indexes obtained using IVIM or other more sophisticated mathematic models may be highly uncertain, erroneous, or even misleading [10]. In the following subsections, we discuss some of the challenges and unresolved issues in adopting more complex analyses of DW-MRI data.

Number and Choice of b Values

To enable perfusion-sensitive information to be gained from DW-MRI, imaging using lower b values (e.g., < 100–200 s/mm^2) is critical. However, there is as yet no consensus on the number of b values that should be used for clinical measurements and the magnitude of b values that should be applied.

The number of b values used for extracting perfusion-sensitive information at DW-MRI varies between studies and ranges from four to more than 10. Because there are four fitted parameters, a minimum of four b values are needed to characterize biexponential signal attenuation, though this choice is not recommended. A larger number of b values would provide more data support for the estimates and, in particular, would enable parameter uncertainties to be evaluated, which is not possible with four b values. Hence, studies utilizing 10 or more b values (combined with least-squares data fitting using a biexponential model) are not unusual in the published literature.

More sophisticated methods for analysis of multiexponential DW-MRI data analysis have been developed [39, 40] and are widely used in the scientific community. These

Fig. 8—65-year-old woman with left transplanted kidney with biopsy-proven type 2 posttransplant rejection. Coronal apparent diffusion coefficient (ADC) map was calculated from diffusion-weighted MRI scans acquired using 10 b values (0–900 s/mm^2). Dysfunctional transplanted kidney (*arrow*) returned lower mean ADC value in renal cortex (1.76×10^{-3} mm^2/s) compared with normal kidneys ($2.03 \times 10^{-3} \pm 0.09 \times 10^{-3}$ mm^2/s, not shown). (Courtesy of Thoeny H, University Bern Inselspital, Bern, Switzerland)

methods can potentially provide more informative analysis than the biexponential approach because the number of exponential components is determined from the data rather than assumed. However, such analysis will only be successful with very high quality data obtained using a large number of b values (e.g., > 10) and multiple signal averages. Because this translates to very long measurement times, this is unlikely to be acceptable to patients or be clinically feasible.

A practical solution is therefore to perform DW-MRI using six to eight b values with several signal averages and to describe the tissue signal attenuation by mathematic model fitting. Because measurements at higher b values have been shown to be relatively stable and reproducible [41], it is theoretically possible to use fewer high b value samplings (e.g., two to three) and acquire more lower b values data (e.g., four or more) to concentrate acquisition time on the more challenging perfusion sensitive range. The choice of b values could potentially be further individualized to the tissue under evaluation, by taking into account the anticipated pattern of signal attenuation with increasing b values and the tissue ADC values [42].

Using multiple b values also affects the choice of DW-MRI technique: free-breathing or respiratory-triggered acquisitions are usually necessary to accommodate multiple b values, although repeated breath-hold examinations using different pairs of b values have also been successfully applied [33]. A typical clinical imaging protocol used to acquire DW-MRI data for IVIM analysis is shown in Table 2.

Confidence in Measurements at Lower b Values

One of the most important challenges to obtaining good biexponential fitting of DW-MRI data are the ability to accurately measure and characterize the tissue signal attenuation at lower b values. From a practical point of view, some MRI platforms do not currently have the flexibility to allow users to specify b values and only fixed values or increments can be chosen, which limits the magnitude and number of lower b values that can be accommodated within the DW-MRI measurement. Future effort is thus required to ensure that all MRI scanners can accurately deliver small b values over any specified set of imaging parameters, field of view, matrix size, and readout gradient. The consistency of this could be quality assured using phantom studies.

Even assuming that lower b values can be freely and accurately prescribed, signal measurements at low b values (e.g., ≤ 100 s/mm^2) are more prone to measurement errors and are highly sensitive to signal-to-noise variations [5, 43], thus posing significant challenges to model fitting. Not surprisingly, it has been found that the reproducibility of ADC values calculated using low b values is poor [41]. There is also a large SD in the estimation of perfusion fraction [35]. For these reasons, voxel-by-voxel analysis may not be appropriate for current IVIM-based evaluation in body DW-MRI, and results generalized over larger regions of interest or across entire target volumes are likely to be more robust. In addition, sophisticated statistic-based data processing could also be performed to both improve fitted results and provide parameter uncertainty estimates [10].

Mathematic Model for Data Fitting

The reader should be aware that the IVIM model represents only one particular description of water diffusion in tissues, which relates the signal attenuation phenomenon observed at low b values to a pseudodiffusion phenomenon, usually ascribed to tissue perfusion. However, as previously discussed, although imaging at low b value is sensitive to tissue vascular perfusion, other secretory physiologic processes in organs may be difficult or impossible to distinguish from vascular perfusion at DW-MRI.

TABLE 2: Typical Scan Parameters Used to Perform Diffusion-Weighted MRI in the Body to Obtain Data for Biexponential Intravoxel Incoherent Motion–Based Analysis

Parameter	Value
MRI platform	1.5-T scanner (Avanto, Siemens Healthcare)
Type of pulse sequence	Single-shot spin-echo echo-planar imaging
Scan orientation	Axial or coronal
Type of acquisition	2D
Respiration	Navigator controlled
TR/TE (ms)	5000/68
Partition thickness (mm)	6
No of partitions	14
Scan coverage	Over target organ or lesion
Matrix	128 × 128
Field of view (mm)	380–450
Phase encode direction	Anterior to posterior
No. of averages	4
Sensitivity encoding factor	Generalized autocalibrating partial parallel acquisition 2
b Values (s/mm^2)	0, 25, 50, 75, 100, 250, 500, and 900
Receiver bandwidth (Hz/pixel)	1780
Fat suppression	Spectral attenuated inversion recovery
Acquisition time	7 min 30 s

TABLE 3: Summary of Mathematic Models Used for Describing Diffusion-Weighted MRI Data

Parameter	Monoexponential	Biexponential (IVIM) [3]	Stretched Exponential [44]	Gaussian [45]	Kurtosis [46]
b Value dependence (S/S_0)	$\exp(-b\,ADC)$	$f\exp(-b\,D^*) + (1-f)\exp(-b\,D)$	$\exp(-(b\,D)^{\alpha})$	$\int p(D)\exp(-b\,D)\,dD$	$\text{Exp}(-b\,D + b^2D^2K/6)$
Summary of terms	ADC = apparent diffusion coefficient (mm^2/s)	f = perfusion fraction (no units); D^* = pseudodiffusion coefficient (mm^2/s); D = diffusion coefficient (mm^2/s)	D = anomalous/distributed diffusion coefficient (mm^2/s); α = subdiffusion exponent; heterogeneity index (no units)	$p(D)$ = truncated gaussian distribution with mode Δ (mm^2/s) and spread σ (mm^2/s).	D = apparent diffusion coefficient (mm^2/s); K = apparent diffusional kurtosis (no units)
Advantages	Simple to estimate, widely available on most scanners.	Accounts for microcapillary perfusion effects, which is known to affect signal attenuation at low b values.	Accounts for more complex diffusion processes. Can be used to fit and derive quantitative estimates of D and α from most datasets.	Accounts for within-voxel heterogeneity. Can be used to fit and derive quantitative estimates from most datasets.	Accounts for more complex diffusion processes.
Disadvantages	Incomplete description of diffusion signal attenuation in the body.	Signal attenuation at low b value may not be specific to perfusion because other bulk flow phenomenon (e.g., fluid flow and glandular secretion) can also attenuate signal. Model may be over-parameterized. Because D^* and f are highly correlated, estimates of D^* may be unreliable. Perfusion effects may not be always be obvious.	Physiologic basis of heterogeneity index is uncertain. Relevance of diffusion model outside the brain for $b < 1000\ mm^2/s$ is uncertain.	Model equation is quite complex and data processing can be slow. Physiologic basis is uncertain.	Model fitting process can be unstable as signal equation *increases* for large b, although measured signal will always *decrease*. Physiologic basis of K is uncertain.

Note—IVIM = intravoxel incoherent motion.

There are also other mathematic models that are currently being explored as descriptors of DW-MRI data. These include a stretched exponential model [44], a gaussian model [45], and a model that includes diffusion and kurtosis (skewness of distribution) [46]. These have been applied to evaluate DW-MRI studies in the brain [47], as well as in the head and neck area [48]. Many models do not directly relate the signal change to a specific physiologic explanation, such as vascular perfusion and tissue diffusivity, but recognize the nonmonoexponential behavior of the diffusion signal attenuation in tissues. A summary of the different models that have been used to describe DW-MRI data in the body is presented in Table 3.

Using the stretched exponential model, for example, the distributed diffusion coefficient and alpha parameters are derived (Fig. 9). Although the distributed diffusion coefficient may be viewed as reflecting tissue diffusivity, interpreting alpha (also known as the heterogeneity index) is less straightforward because there is no direct physiologic underpinning for this parameter. Thus, even though alpha has been shown to change with treatment in tumors [47], there is currently no clear link between the parameter and a pathophysiologic explanation, and thus its potential to be a true biomarker has yet to be established. Nevertheless, the current evidence suggests that alpha and other parameters may be useful as statistical markers of disease, but until their biologic relevance is understood, it is essential that this distinction is clear and articulated by practitioners.

From the foregoing discussion, it perhaps comes as no surprise that the IVIM model remains the most popular approach to explore nonmonoexponential DW-MRI signal attenuation in tissues. Although IVIM has a biologic interpretation for the observations, it may not always provide the most concise description for acquired data. Consequently, the most appropriate compromise between applying the biologically relevant IVIM model that may be a suboptimal descriptor for the data versus using other models that provide a better mathematic fit but have uncertain biologic significance has yet to be established (Fig.

Fig. 9—Diffusion-weighted MRI data for liver and right kidney in 45-year-old man, fitted using mathematic models. Plots (*circles*) of mean logarithm of relative signal intensities versus b values are shown. Same data points for each organ can be described using biexponential intravoxel incoherent motion (IVIM)–based model (*black line*) but may also be described using other mathematic models that make different assumptions about signal attenuation behavior (e.g., stretched exponential, *gray line*). In liver, data points are better characterized using IVIM-based analysis. However, in kidney, both IVIM and stretched exponential models provide very close descriptions of data.

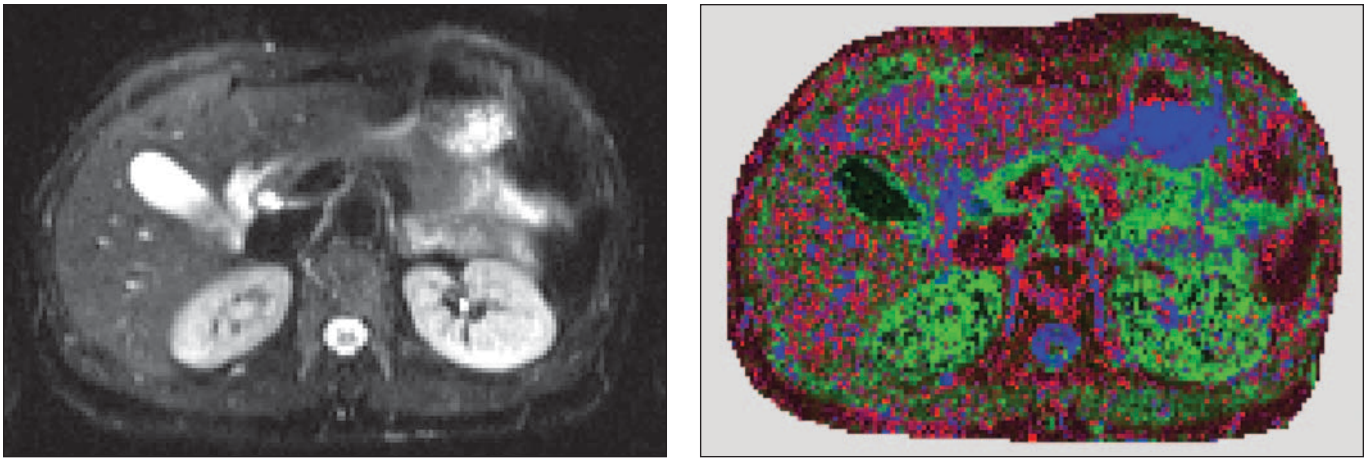

Fig. 10—25-year-old healthy woman who underwent axial diffusion-weighted (DW) MRI using navigator-controlled spin-echo echo-planar imaging with 10 b values (0, 25, 50, 75, 100, 150, 250, 500, 750, and 900 s/mm^2).
A, Axial DW-MRI of upper abdomen (b = 0 s/mm^2) is shown.
B, Colorized map shows, on voxel-by-voxel basis, probability that each model best describes signal attenuation data (strong colors indicate high probability, and mixed colors represent model ambiguity; black = monoexponential, red = stretched exponential, blue = intravoxel incoherent motion biexponential, and green = gaussian). Note considerable heterogeneity of signal attenuation pattern in tissues, indicating challenges in generalizing such behavior to region of interest or to whole organ.

9). Even allowing a wider application of the IVIM model, the best way to derive the diffusion coefficient, pseudodiffusion coefficient, and perfusion fraction from acquired data is still being explored. Because pseudodiffusion coefficient and perfusion fraction parameters are highly correlated, one approach would be to fix the pseudodiffusion coefficient value using a priori information [33].

The situation is potentially even more complex because of heterogeneous patterns of signal attenuation on a voxelwise basis in normal tissues and tumors. By way of an illustrative example (Fig. 10), a voxel within a tissue may exhibit signal attenuation best described by the IVIM model, but adjacent voxels may show signal loss best described by other models. The difficulty in generalizing such behavior to a region of interest is indeed challenging, because choosing to fit all voxels in a region to one model can result in approximation. Clearly, future studies should aim to improve our understanding of the biologic relevance of a range of mathematic models and developing novel algorithms to describe complex DW-MRI tissue behavior [10].

Software for Data Analysis

Currently, most commercial MRI platforms cannot perform complex analysis of DW-MRI data. However, vendors are interested in introducing more sophisticated analytic techniques onto their imaging platforms. IVIM-based analysis is currently possible with the appropriate technical support or through the use of third-party software. Nevertheless, the repeatability and usefulness of the nonmonoexponential model–derived parameters still need to be established and improved in larger prospective studies, so that these may be meaningfully applied.

Conclusion

DW-MRI performed using a range of low and high b values can allow estimates of tissue perfusion and diffusivity to be made by IVIM-based analysis. Clinical studies have shown the potential value of such parameters for disease assessment, particularly in oncology. However, it should be recognized that, although the fast diffusion component suppressed using low b values is sensitive to microcapillary perfusion, other bulk flow phenomena such as tubular flow or glandular secretion can contribute to the signal attenuation and may be difficult to distinguish from perfusion effects.

Radiologists should be aware that there are still significant challenges in implementing more complex quantitative DW-MRI analysis and there are uncertainties associated with such approaches. Robust DW-MRI data analysis beyond simple monoexponential ADC evaluation is not straightforward, requiring high-quality data acquired using multiple b values and confidence in the measurements at low b values. Even when these conditions are met, the choice and execution of the mathematic models remains a complex issue. Future work should be directed at these challenges to enable more sophisticated diffusion quantitative parameters to be developed as biomarkers.

References

1. Koh DM, Collins DJ. Diffusion-weighted MRI in the body: applications and challenges in oncology. *AJR* 2007; 188:1622–1635
2. Takahara T, Imai Y, Yamashita T, Yasuda S, Nasu S, Van Cauteren M. Diffusion weighted whole body imaging with background body signal suppression (DWIBS): technical improvement using free breathing, STIR and high resolution 3D display. *Radiat Med* 2004; 22:275–282
3. Le Bihan D, Breton E, Lallemand D, Grenier P, Cabanis E, Laval-Jeantet M. MR imaging of intravoxel incoherent motions: application to diffusion and perfusion in neurologic disorders. *Radiology* 1986; 161:401–407
4. Le Bihan D, Breton E, Lallemand D, Aubin ML, Vignaud J, Laval-Jeantet M. Separation of diffusion and perfusion in intravoxel incoherent motion MR imaging. *Radiology* 1988; 168:497–505
5. Le Bihan D, Turner R, Moonen CT, Pekar J. Imaging of diffusion and microcirculation with gradient sensitization: design, strategy, and significance. *J Magn Reson Imaging* 1991; 1:7–28
6. Le Bihan D. IVIM method measures diffusion and perfusion. *Diagn Imaging (San Franc)* 1990; 12:133–136
7. Le Bihan D. Intravoxel incoherent motion perfusion MR imaging: a wake-up call. *Radiology* 2008; 249:748–752
8. Bammer R. Basic principles of diffusion-weighted imaging. *Eur J Radiol* 2003; 45:169–184
9. Stejskal EO, Tanner JE. Spin diffusion measure-

ments: spin-echo in the presence of a time dependent field gradient. *J Chem Phys* 1965; 42:288–292

10. Neil JJ, Bretthorst GL. On the use of Bayesian probability theory for analysis of exponential decay data: an example taken from intravoxel incoherent motion experiments. *Magn Reson Med* 1993; 29:642–647
11. Sakuma H, Tamagawa Y, Kimura H, et al. Intravoxel incoherent motion (IVIM) imaging using an experimental MR unit with small bore (in Japanese). *Nippon Igaku Hoshasen Gakkai Zasshi* 1989; 49:941–943
12. Sun X, Wang H, Chen F, et al. Diffusion-weighted MRI of hepatic tumor in rats: comparison between in vivo and postmortem imaging acquisitions. *J Magn Reson Imaging* 2009; 29:621–628
13. Neil JJ, Bosch CS, Ackerman JJ. An evaluation of the sensitivity of the intravoxel incoherent motion (IVIM) method of blood flow measurement to changes in cerebral blood flow. *Magn Reson Med* 1994; 32:60–65
14. Henkelman RM, Neil JJ, Xiang QS. A quantitative interpretation of IVIM measurements of vascular perfusion in the rat brain. *Magn Reson Med* 1994; 32:464–469
15. Wang Z, Su MY, Najafi A, Nalcioglu O. Effect of vasodilator hydralazine on tumor microvascular random flow and blood volume as measured by intravoxel incoherent motion (IVIM) weighted MRI in conjunction with Gd-DTPA-albumin enhanced MRI. *Magn Reson Imaging* 2001; 19: 1063–1072
16. Pickens DR 3rd, Jolgren DL, Lorenz CH, Creasy JL, Price RR. Magnetic resonance perfusion/diffusion imaging of the excised dog kidney. *Invest Radiol* 1992; 27:287–292
17. Lemke A, Laun FB, Simon D, Stieltjes B, Schad LR. An in vivo verification of the intravoxel incoherent motion effect in diffusion-weighted imaging of the abdomen. *Magn Reson Med* 2010; 64: 1580–1585
18. Henkelman RM. Does IVIM measure classical perfusion? *Magn Reson Med* 1990; 16:470–475
19. Le Bihan D, Turner R. The capillary network: a link between IVIM and classical perfusion. *Magn Reson Med* 1992; 27:171–178
20. Wirestam R, Borg M, Brockstedt S, Lindgren A, Holtas S, Stahlberg F. Perfusion-related parameters in intravoxel incoherent motion MR imaging compared with CBV and CBF measured by dynamic susceptibility-contrast MR technique. *Acta Radiol* 2001; 42:123–128
21. Powers TA, Lorenz CH, Holburn GE, Price RR. Renal artery stenosis: in vivo perfusion MR imaging. *Radiology* 1991; 178:543–548
22. Patel J, Sigmund EE, Rusinek H, Oei M, Babb JS, Taouli B. Diagnosis of cirrhosis with intravoxel incoherent motion diffusion MRI and dynamic contrast-enhanced MRI alone and in combination: preliminary experience. *J Magn Reson Imaging* 2010; 31:589–600
23. Yoshino N, Yamada I, Ohbayashi N, et al. Salivary glands and lesions: evaluation of apparent diffusion coefficients with split-echo diffusion-weighted MR imaging—initial results. *Radiology* 2001; 221:837–842
24. Zhang L, Murata Y, Ishida R, Ohashi I, Yoshimura R, Shibuya H. Functional evaluation with intravoxel incoherent motion echo-planar MRI in irradiated salivary glands: a correlative study with salivary gland scintigraphy. *J Magn Reson Imaging* 2001; 14:223–229
25. Muller MF, Prasad PV, Edelman RR. Can the IVIM model be used for renal perfusion imaging? *Eur J Radiol* 1998; 26:297–303
26. Thoeny HC, De Keyzer F, Oyen RH, Peeters RR. Diffusion-weighted MR imaging of kidneys in healthy volunteers and patients with parenchymal diseases: initial experience. *Radiology* 2005; 235:911–917
27. Ries M, Jones RA, Basseau F, Moonen CT, Grenier N. Diffusion tensor MRI of the human kidney. *J Magn Reson Imaging* 2001; 14:42–49
28. Chow LC, Bammer R, Moseley ME, Sommer FG. Single breath-hold diffusion-weighted imaging of the abdomen. *J Magn Reson Imaging* 2003; 18: 377–382
29. Yang D, Ye Q, Williams DS, Hitchens TK, Ho C. Normal and transplanted rat kidneys: diffusion MR imaging at 7 T. *Radiology* 2004; 231:702–709
30. Riches SF, Hawtin K, Charles-Edwards EM, de Souza NM. Diffusion-weighted imaging of the prostate and rectal wall: comparison of biexponential and monoexponential modelled diffusion and associated perfusion coefficients. *NMR Biomed* 2009; 22:318–325
31. Mulkern RV, Barnes AS, Haker SJ, et al. Biexponential characterization of prostate tissue water diffusion decay curves over an extended b-factor range. *Magn Reson Imaging* 2006; 24:563–568
32. Shinmoto H, Oshio K, Tanimoto A, et al. Biexponential apparent diffusion coefficients in prostate cancer. *Magn Reson Imaging* 2009; 27:355–359
33. Lemke A, Laun FB, Klau M, et al. Differentiation of pancreas carcinoma from healthy pancreatic tissue using multiple b-values: comparison of apparent diffusion coefficient and intravoxel incoherent motion derived parameters. *Invest Radiol* 2009; 44:769–775
34. Yamada I, Aung W, Himeno Y, Nakagawa T, Shibuya H. Diffusion coefficients in abdominal organs and hepatic lesions: evaluation with intravoxel incoherent motion echo-planar MR imaging. *Radiology* 1999; 210:617–623
35. Koh DM, Scurr E, Collins DJ, et al. Colorectal hepatic metastases: quantitative measurements using single-shot echo-planar diffusion-weighted MR imaging. *Eur Radiol* 2006; 16:1898–1905
36. Thoeny HC, Zumstein D, Simon-Zoula S, et al. Functional evaluation of transplanted kidneys with diffusion-weighted and BOLD MR imaging: initial experience. *Radiology* 2006; 241:812–821
37. Eisenberger U, Thoeny HC, Binser T, et al. Evaluation of renal allograft function early after transplantation with diffusion-weighted MR imaging. *Eur Radiol* 2010; 20:1374–1383
38. Zhang JL, Sigmund EE, Chandarana H, et al. Variability of renal apparent diffusion coefficients: limitations of the monoexponential model for diffusion quantification. *Radiology* 2010; 254:783–792
39. Provencher SW. A Fourier method for the analysis of exponential decay curves. *Biophys J* 1976; 16:27–41
40. Pfeuffer J, Provencher SW, Gruetter R. Water diffusion in rat brain in vivo as detected at very large b values is multicompartmental. *MAGMA* 1999; 8:98–108
41. Koh DM, Blackledge M, Collins DJ, et al. Reproducibility and changes in the apparent diffusion coefficients of solid tumours treated with combretastatin A4 phosphate and bevacizumab in a two-centre phase I clinical trial. *Eur Radiol* 2009; 19:2728–2738
42. Blackledge M, Collins DJ. Technique and optimization. In: Koh DM, Thoeny H, eds. *Diffusion-weighted MR imaging: applications in the body.* Heidelberg: Springer-Verlag, 2010
43. Pekar J, Moonen CT, van Zijl PC. On the precision of diffusion/perfusion imaging by gradient sensitization. *Magn Reson Med* 1992; 23:122–129
44. Bennett KM, Schmainda KM, Bennett RT, Rowe DB, Lu H, Hyde JS. Characterization of continuously distributed cortical water diffusion rates with a stretched-exponential model. *Magn Reson Med* 2003; 50:727–734
45. Yablonskiy DA, Bretthorst GL, Ackerman JJ. Statistical model for diffusion attenuated MR signal. *Magn Reson Med* 2003; 50:664–669
46. Jensen JH, Helpern JA, Ramani A, Lu H, Kaczynski K. Diffusional kurtosis imaging: the quantification of non-gaussian water diffusion by means of magnetic resonance imaging. *Magn Reson Med* 2005; 53:1432–1440
47. Kwee TC, Galban CJ, Tsien C, et al. Intravoxel water diffusion heterogeneity imaging of human high-grade gliomas. *NMR Biomed* 2010; 23:179–187
48. Jansen JF, Stambuk HE, Koutcher JA, Shukla-Dave A. Non-gaussian analysis of diffusion weighted MRI in head and neck cancer: a feasibility study. In: *17th annual meeting of the International Society of Magnetic Resonance in Medicine.* Berkeley, CA: International Society of Magnetic Resonance in Medicine, 2009
49. Luciani A, Vignaud A, Cavet M, et al. Liver cirrhosis: intravoxel incoherent motion MR imaging—pilot study. *Radiology* 2008; 249:891–899